PAPER • OPEN ACCESS

The effect of APC/YBCO interface on the angular range of effective pinning by one-dimensional artificial pinning centers in $YBa_2Cu_3O_{7-x}$ nanocomposite films

The effect of APC/YBCO interface on the angular range of effective pinning by one-dimensional artificial pinning centers in YBa₂Cu₃O₇₋ₓ nanocomposite films

V Ogunjimi[1], B Gautam[1], M. A. Sebastian[2,3], T Haugan[2], J Wu[1]

[1]*Department of Physics and Astronomy, the University of Kansas, Lawrence, Kansas 66045,USA*
[2]*U.S Air Force Research Laboratory, Aerospace Systems Directorate, WPAFB, OH 45433, USA*
[3]*University of Dayton Research Institute, Dayton, OH 45469, USA*

E-mail: jwu@ku.edu; and victorogunjimi@ku.edu

Abstract. The APC/YBCO interface has been reported to directly affect the pinning efficiency of 1D APCs at $B//c$-axis. This raises a question on how the APC/YBCO interface affects angular range of the pinning effectiveness for a given 1D APC. In this work, two types of 1D APCs of different APC/YBCO interfaces and hence pinning efficiencies were selected to understand the correlation of the pinning efficiency at $B//c$-axis and the angular range of the effectiveness. Specifically, $BaZrO_3$ (BZO) and $BaHfO_3$ (BHO) 1D APCs were selected for a comparative study in the APC/YBCO nanocomposite films. The BZO and BHO 1D APCs have comparable diameters in the range of 5-6 nm. In the doping range of 2-6 vol.%, both BZO and BHO form c-axis aligned 1D APCs in YBCO films. However, differences are present at their interfaces with YBCO. While the BZO/YBCO interface is semi-coherent, a coherent BHO/YBCO interface has been found to be critical to the higher pinning efficiency of the BHO 1D APCs. Therefore, they provide ideal systems for investigation of the angular range of pinning effectiveness by 1D APCs. By evaluating the nanocomposites' maximum pinning force density ($F_{p, max}$) and its location B_{max}, normalized to that of the reference YBCO film as functions of magnetic field (B) orientation at temperatures of 65–77 K, a quantitative correlation between the pinning efficiency of the BZO 1D-APCs and their effective angular range was obtained. Our results indicate that all 1D APCs can provide enhanced B_{max} over certain angular ranges away from the c-axis. However, 1D APCs with higher pinning efficiency, such as BHO 1D APCs can have enhanced $F_{p, max}$ over the entire angular range of B-orientations at temperatures of 65-77 K with respect to that for the reference YBCO sample.

1. Introduction

Nanoscale artificial pinning centers (APCs) in YBa₂Cu₃O₇₋ₓ (YBCO) and other high T_c superconducting films on various substrates have been reported to enhance magnetic vortex pinning and hence critical current density J_c in applied magnetic fields (B) [1-7]. Most APCs form through addition of secondary dopants like $BaZrO_3$ (BZO), $BaHfO_3$ (BHO) and other insulator oxides that aggregate into APCs via strain mediated self-assembly in APC/YBCO nanocomposites during growth [8]. In particular, c-axis

aligned one-dimensional APCs (1D-APCs) have been reported to provide strong correlated pinning in YBCO nanocomposites at B//c-axis [5-7, 9-18]. Since 1D-APCs are expected to be effective within a limited angular range around B//c-axis, investigating how this angular range is affected by APC materials is crucial to achieving an optimal strong and B-field orientation-independent pinning landscape for practical applications.

BZO and BHO both form c-axis aligned 1D-APCs in YBCO nanocomposites with comparable diameters in the range of 5-6 nm. However, the BZO 1D-APC/YBCO and BHO 1D-APC/YBCO interfaces differ considerably due to the difference in the lattice mismatches and elastic properties of the materials involved, which result in differences in the microstructures and pinning efficiencies of the two types of the 1D-APCs [19, 20]. Specifically, the BZO 1D-APC/YBCO interface is semi-coherent with a high concentration of defects such as dislocations in a YBCO column of a few nm in thickness around the BZO 1D-APC [21]. While the local strain is significantly reduced in the column with respect to the theoretical values based on the BZO/YBCO lattice mismatch, oxygen deficiency has been revealed as a consequence of the defects. Therefore, a lower interface T_c in this YBCO column as compared to the global T_c of the nanocomposite can be projected, which can lead to a reduced pinning potential across the BZO 1D-APC/YBCO interface. In contrast, the BHO 1D-APC/YBCO interface can be made approximately coherent with much reduced defect concentration and hence less degraded interface T_c in the YBCO column around the BHO 1D-APC [20]. This explains the significantly higher pinning efficiency of the BHO 1D-APC as compared to its BZO counterpart at B//c-axis in terms of high pinning force density ($F_p(B) = J_c \times B$), especially the peak value ($F_{p, max}$) and its location (B_{max}) [20].

Considering the correlated pinning by c-axis aligned 1D-APCs is typically illustrated as a peak of J_c as function of the B orientation in the plane perpendicular to the J_c, defined using angle θ with θ=0 for B//c-axis *and* θ=90° for B//ab-plane, a question arises on how the angular range of the 1D-APC pinning correlates with the pinning efficiency of the 1D-APCs. In fact, many previous studies have investigated $J_c(\theta)$ on various nanocomposites including BZO and BHO ones [22-34]. This work adopts a slightly different approach by measuring $J_c(B)$ and $F_p(B)$ at θ angles. This allows extraction of the $F_{p, max}(\theta)$ and $B_{max}(\theta)$ on BZO and BHO 1D-APC/YBCO nanocomposite films. By plotting these values normalized to that of reference YBCO film, we aim to shed light on the effect of the 1D-APC pinning efficiency on the angular range the correlated pinning extends.

2. Experimental

2 vol.% and 4 vol. % singly doped BZO/YBCO and BHO/YBCO nanocomposite films (to be regarded henceforth as 2% BZO, 4% BZO, 2% BHO and 4% BHO) and a reference YBCO film were selected for this study. The samples were fabricated using pulse laser deposition (PLD) technique on (100) SrTiO₃ (STO) single crystal substrates under optimal PLD conditions. The fabrication details have been reported elsewhere [20, 34, 35]. Briefly, the substrate temperatures of 825 °C and 810 °C, respectively,
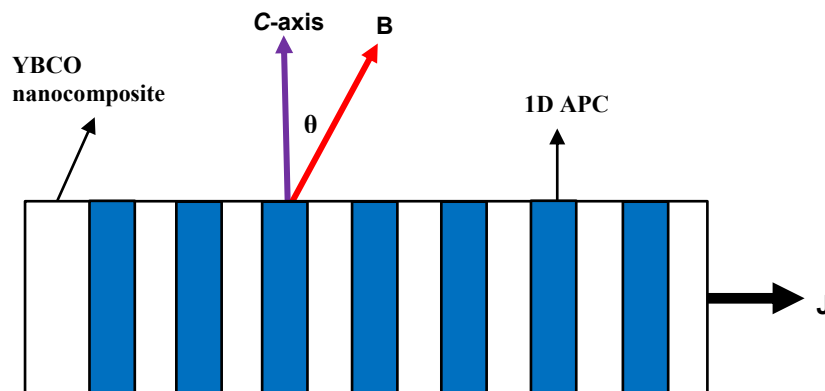

Figure 1. Schematic showing the deviation angle θ of the magnetic field, B away from the c-axis of APC/YBCO nanocomposite films and the direction of the electric current in the film.

were employed for PLD BZO and BHO 1D-APC/YBCO nanocomposite films in 300 mTorr oxygen using a Lambda Physik LPX 300 KrF excimer laser (248 nm). The laser energy density and repetition frequency were set at 1.6 J/cm^2 and 8.0 Hz respectively. The samples were in situ annealed in oxygen for 30 minutes at 500°C. The sample thickness is around 140 nm and silver contacts were sputtered on all samples after the PLD growth. The crystallinity and microstructure of these samples were reported in our previous works [9, 20, 36, 37]. The samples are all c-axis oriented epitaxial films. In all nanocomposite samples, c-axis aligned 1D-APCs have been confirmed with BZO 1D-APC diameter in range of 5.2-5.7 nm and BHO 1D-APC diameter around 5.0 nm. The T_c values are 89.27 K, 87.48 K, 89.36 K and 87.40 K for 2% BZO, 4% BZO, 2% BHO and 4% BHO respectively. Two microbridges of length 500 µm and widths of 20 µm and 40 µm were patterned on each sample using photolithography. The samples were wired to pins on a sample stage with 50 µm in diameter platinum wires. This stage rotation was done in the plane perpendicular to the $J_c(B)$ as depicted schematically in Figure 1 at different angles such that the applied B field orientation angle with respect to the c-axis, θ, can be varied from $\theta \sim 0°$ to $\theta \sim 90°$. J_c was determined using the 1 µVcm^{-1} criterion Specifically for this work, $J_c(B)$ measurements were carried out in a Physical Property Measurement Systems (Evercool II, Quantum Design) at 65 and 77 K with B up to 9 T and at several selected θ angles between 0° ($B//c$-axis) and 90° ($B//ab$-plane). $F_p(B) = J_c \times B$ curves were then derived from the measured $J_c(B)$ curves at these θ angles for analyses.

3. Results

Figure 2 depicts the $F_p(B)$ curves taken on the reference YBCO (Figures 2a-b), 2% BZO (Figures 2c-d) and 4% BZO SD (Figures 3e-f) nanocomposite samples at different θ angles of 0°, 22°, 37°, 45°, 67° and 90°. These θ angles were selected based on a preliminary test to ensure the difference between the $F_p(B)$ curves at these angles are well distinguishable. It should be noted that the B_{max} values may be above the limit of experimental apparatus of 9.0 T on some $F_p(B)$ curves in this work, such as the 4% BHO/YBCO sample at 65 K. In this case, B_{max} is assigned the value of 9.0 T as the lower limit. In the reference YBCO sample, the intrinsic pinning by the ab-planes provides the strongest pinning at $B//ab$ ($\theta = 90°$) as expected at both 77K and 65 K. This is illustrated in the highest $F_p(B)$ at $\theta = 90°$ and decreasing $F_p(B)$ with decreasing θ angles. The 77 K behavior shows the 90° pinning force clearly over performing the other orientations. At 65 K, this trend persists although the difference in $F_p(B)$ curves at different θ angles is narrowed in the B-field range of 0-9 T. In the 2% BZO sample (Figures 2c-d), the addition of the c-axis aligned 1D-APCs is demonstrated in the enhanced $F_p(B)$ at $\theta = 0°$ and other smaller θ angles as compared to that in the reference YBCO, although the $F_p(B)$ at $\theta = 90°$ remains similar to that of YBCO. Quantitatively, the pinning efficiency of the BZO 1D-APCs differs at different temperatures. At 77 K, the enhancement in F_p is moderate while at 65 K, greater $F_{p, max}$ enhancement is seen at 0° and 22°. In contrast, as the BZO doping is increased to 4% (Figure 2e-f), the $F_p(B)$ at these two field orientations outperform that at $\theta = 90°$ and other angles. At 77 K, the $F_{p, max}$ at $\theta = 0°$ (circle) and 22° (square) $\sim$ 13.3 and $\sim$ 10.8 GN/m^3 respectively compared to only about $\sim$ 6 GN/m^3 or lower for other angles. In addition, due to stronger correlated pinning in this sample its $F_{p, max}$ at $\theta = 90°$ underperforms those at these two orientations. The results indicate that in terms of pinning enhancement relative to the reference YBCO sample, the 4% BZO sample exhibits the best performance. Specifically, for $\theta < 67°$, the pinning enhancement by the BZO 1D APCs in the 2% BZO sample (relative to YBCO) is only illustrated in a shift of the B_{max} to $\sim$ 3.0 T from $\sim$ 2.0 T in the YBCO reference sample. The performance of 4% BZO over 2% BZO may be attributed to the enhanced strain field overlap in the 4% BZO sample. Enhanced strain field overlap results in the formation of larger number of defects density in the 4% BZO. These defects reduce the strain in the BZO/YBCO interface thereby minimizing the formation of oxygen vacancies in the interface.

Figures 3 compares the $F_p(B)$ curves measured at θ angles of 0º, 45º and 90º for 2% BZO 1D-APC/YBCO (solid) and BHO 1D-APC/YBCO (open) nanocomposites at 77 K and 65 K (Figures 3a-3b), and for 4% counterparts at the same temperatures (Figures 3c-3d), respectively. For both 2% and 4% APC doping cases, the $F_{p,\,max}$ at $\theta =0^o$ of the BHO samples are significantly higher than that of the
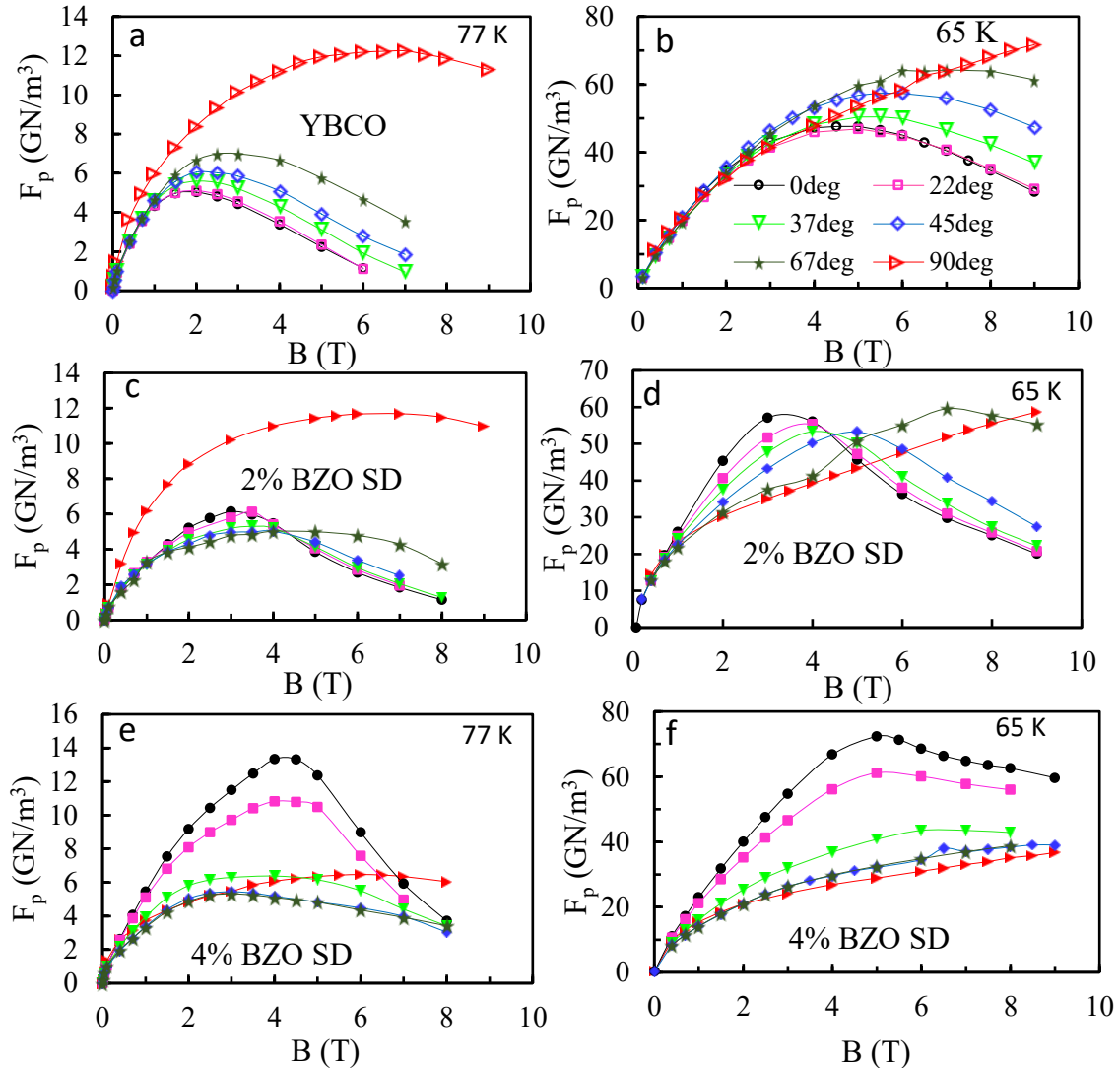

Figure 2. $F_P(B)$ curves for each θ measured at 77 K (solid symbols) and 65 K (open symbols) on 2% BZO SD (a and b), 4% BZO SD (c and d), and undoped YBCO (e and f).

BZO samples. For instance, the $F_{p,\,max}$ values of the 2% BHO sample are 12.9 GN/m^3 and 76.9 GN/m^3 at 77 K and 65 K respectively. These values are significantly higher than the $F_{p,\,max}$ values of 6.1 GN/m^3 at 77 K and 57.1 GN/m^3 at 65 K for the 2% BZO sample. The superior performance in the BHO sample is even more remarkable when the 4% samples are compared at 65 K. At this lower temperature, the $F_{p,\,max}$ value of 182.3 GN/m^3 at $\theta =0^o$ for the 4% BHO sample is about two and half times the value of its BZO counterpart. This strong correlated pinning by the BHO 1D-APCs may be ascribed to its coherent BHO/YBCO interface [20]. The lower (relative to BZO) lattice mismatch of the BHO with YBCO may ensure less interfacial dislocations and lower oxygen vacancy density around the BHO/YBCO interface. The difference in $F_p(B)$ magnitude of the samples is less dramatic at 45º and 77 K. Nevertheless, the BHO 1D-APCs are still more effective at this orientation and temperature as shown in Figures 3a and 3c. At 65 K, the $F_p(B)$ curve of 4% BHO at $\theta =45^o$ is consistently higher at all fields than that of 4% BZO (Figure 3d). Interestingly, the $F_{p,\,max} \sim 94.9\ GN/m^3$ in the 4% BHO is not only more than double of
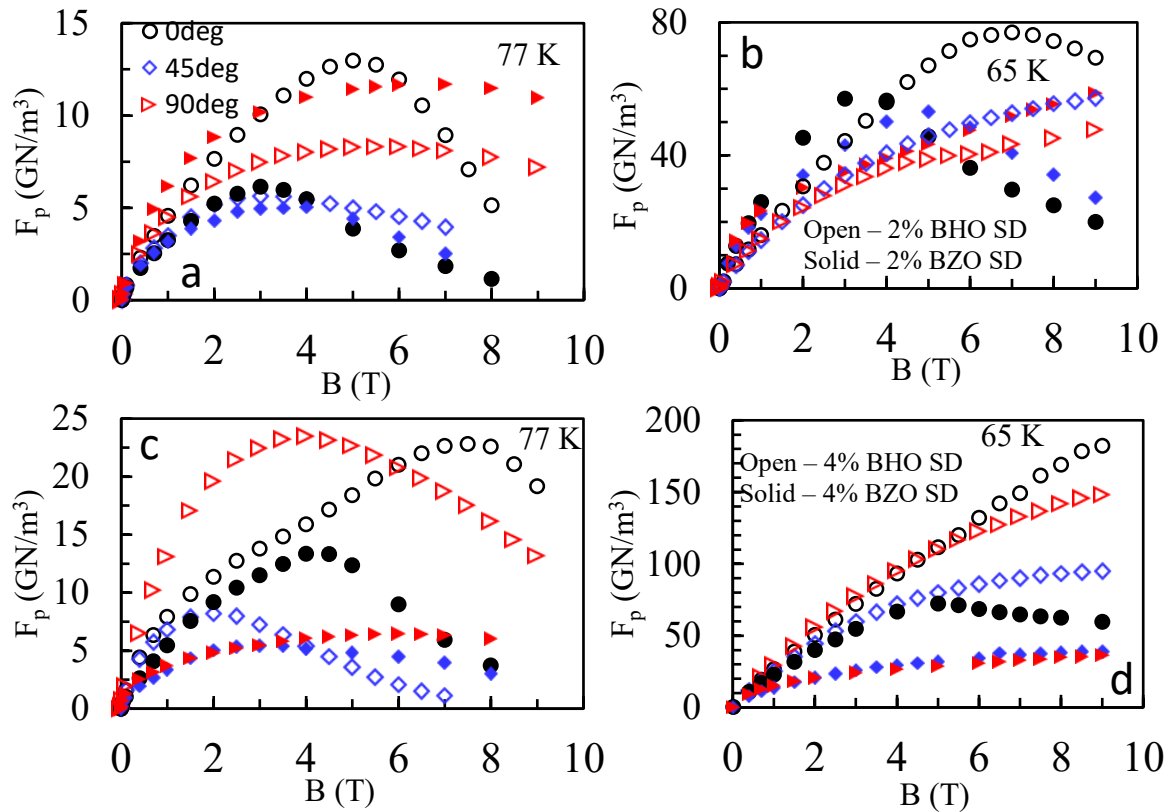
Figure 3. Comparison of the $F_P(B)$ curves of) (a and b) 2% BHO SD (open) and 2% BZO SD (solid); and (c and d) 4% BHO SD (open) and 4% BZO SD (solid) at 77 K and 65 K.

that of the 4% BZO film, it is also higher than the BZO sample's $F_{p, max}$ at $\theta = 0^o$. In fact, while the $F_p(B)$ curve of the 4% BHO sample at $\theta = 45^o$ is comparable to that of the 4% BZO's below 5.0 T, beyond this field, it continues increasing with B-field, in contrast to the decreasing trend for the BZO sample at higher fields. In other words, at the same doping level, the BHO 1D-APCs are stronger pins at 45° than the BZO 1D-APCs at $B//c$. This behaviour points to a relatively wider angular range of the pinning enhancement in the BHO sample. The $F_p(B)$ trend of the nanocomposite samples is bifurcated at $\theta = 90^o$. The $F_{p, max}$ values in 2% BZO of 11.7 (77 K) and 58. 7 GN/m^3 (65 K) are slightly higher than that measured in the 2% BHO film. However, the 4% BHO values of 23.5 (77 K) and 148.5 GN/m^3 (65 K) are about quadrupled the results from the 4% BZO films. It is also important to note that the $F_{p, max}$ values of 12.3 (77 K) and 71.7 GN/m^3 (65 K) at $\theta = 90^o$ measured on the reference YBCO (Figures 2e – 2f) are significantly smaller than those of the 4% BHO film [20].

The angular range of the effective pinning by the BZO and BHO 1D-APCs is quantified by the $F_{p, max}$ (Figures 4a-4b) and B_{max} (Figures 4c–4d) values of the nanocomposite films normalized to that of the reference YBCO film as functions of θ at 77 K (solid symbols) and 65 K (open symbols). At both temperatures, enhanced $F_{p, max}$ is observed for all four nanocomposite samples at lower angles up to $\theta \sim$ 40° except the 4% BHO sample that shows enhancement in the entire angular range up to $\theta \sim 90^o$. The amplitude of the $F_{p, max}$ enhancement is the highest at $\theta = 0^o$ and decreases monotonically with increasing θ. Differing from the trend that the normalized $F_{p, max}$ is smaller than 1 (or worse than that of YBCO) at $\theta > 40^o$ for the other three samples, the normalized $F_{p, max}$ for the 4% BHO nanocomposite exhibits a second peak at $\theta = 90^o$, which is indicative of the benefit of high pinning efficiency associated to the coherent BHO/YBCO interface. At 77 K, the data show the amplitude of the $F_{p, max}$ enhancement of 2% BZO going below the reference YBCO value at $\sim 37^o$ while those of the 4% BZO and 2% BHO fall below 1 at $\sim 37^o$. At 65 K the point at which the amplitude crosses the reference line has contracted to
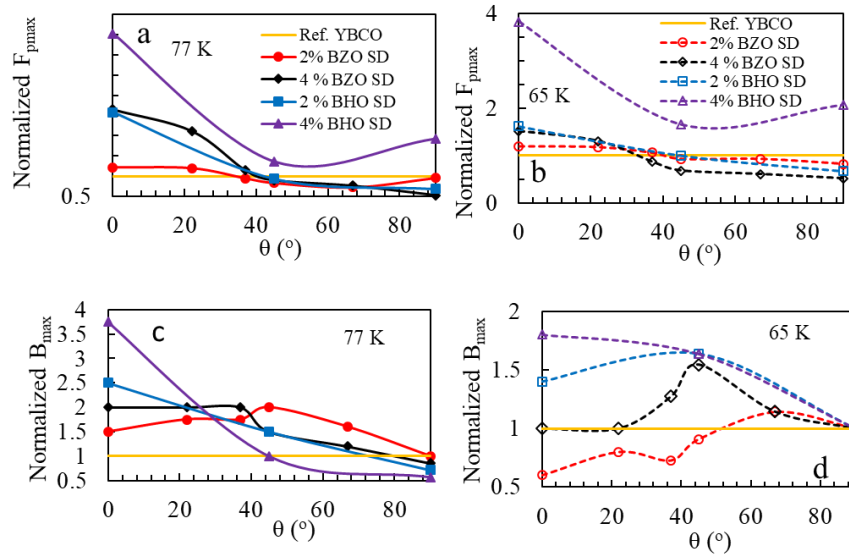
Figure 4. The ratio of $F_{p, max}$ (a and b) and B_{max} (c and d) to reference YBCO values vs θ at 77 K (solid symbols) and 65 K (open symbols) for the samples- 2% BZO SD (circle), 4 % BZO SD (diamond), 2% BHO SD (square) and 4 % BHO SD (triangle) with Ref. YBCO (horizontal line).

less than ~ 37° in the 4% BZO and remains roughly same for the 2% samples. The highest normalized $F_{p, max}$ up to 4.53 is observed in the 4% BHO at 77 K followed by ~ 2.6 in the 4% BZO and 2% BHO sample at the same temperature. This result suggests that in terms of correlated pinning and the angular range of pinning, the 2% BHO is comparable to the 4% BZO. Doubling the BHO concentration to 4% almost doubles the correlated pinning and extends the angular range to ~ 90°. This might be connected to the coherent BHO/YBCO interface. Perhaps, the coherent interface provides such a strong correlated pinning that some of pinning benefits at $B//c$ are extended to other orientations. The normalized B_{max} data show that at 77 K, all samples (except 4% BHO) show enhancement up to about 67°. At 65 K the trends of the amplitude of the normalized B_{max} of the BHO films differ from (and are significantly higher than) those of the BZO samples across the angular window. In the 2% BHO film, the amplitude increases from ~ 1.4 at 0° until it reaches a maximum at 45° and decreases monotonically until it crosses the reference value at 90°. The 4% BHO also goes below the YBCO value at ~ 90° except its maximum is at 0° and it decreases monotonically with increasing θ. However, while both BZO films show a smaller normalized B_{max} and narrower B_{max} enhancement range, only the 2% BZO records negative B_{max} enhancement (between 0° and 45°). The amplitude of the B_{max} enhancement of the 2% BZO reaches a peak at about 67° then decreases to YBCO level at 90°. The amplitude of the 4% BZO stays at 1 until ~ 22° then increases and attains a maximum at ~ 45° before falling monotonically.

4. Conclusion

In summation, $F_p(B)$ curves were studied at selected B-orientations on 2% and 4% BZO and BHO doped 1D-APC/YBCO nanocomposite films at 65 K and 77 K. To quantify the B-orientation range of the enhanced pinning by the 1D-APCs, the $F_{p,max,}$ and B_{max} normalized to that of the reference YBCO film were plotted as functions of θ. Several important observations have been made in this comparative study on BZO and BHO 1D-APCs of different interfaces with YBCO. It has been found that the pinning benefit of the c-axis aligned 1D-APCs extends beyond $\theta=0°$ ($B//c$-axis) as shown in both the normalized $F_{p,max,}$ and B_{max} exceeding 1. Quantitatively, the enhancement and angular range vary with APC concentrations and APC/YBCO interface quality. The enhanced B_{max} up to ~ 67° was observed in all the nanocomposite films with the BHO samples exhibiting remarkable B_{max} enhancement especially at 65 K. In particular, the $F_{p,max,}$ enhancement angular range correlates well with the pinning efficiency of the 1D-APCs and the highest $F_{p,max,}$ enhancement over the entire θ range has been observed in the 4% BHO 1D-APCs/YBCO nanocomposite sample. This result has therefore revealed interesting correlation between the pinning efficiency of the 1D-APCs, which is dictated by the quality of the APC/YBCO interface and the H-orientation angular range, which is important to further improvement of pinning landscape.

References

[1]   Larbalestier, D et al., *High-Tc superconducting materials for electric power applications.* Nature, 2001. **414**(6861): p. 368-377.

[2]   Malozemoff, A P *High Tc for the power grid.* Nature Materials, 2007. **6**(9): p. 617-619.

[3]   Luongo, C A et al., *Next Generation More-Electric Aircraft: A Potential Application for HTS Superconductors.* IEEE Transactions on Applied Superconductivity, 2009. **19**(3): p. 1055-1068.

[4]   Holtz, R.L., et al., *High Temperature Superconductors for Naval Power Applications.* Materials Science and Technology: 2006 NRL Review, 2006: p. 1-3.

[5]   Obradors, X., et al., *Growth, nanostructure and vortex pinning in superconducting YBa2Cu3O7 thin films based on trifluoroacetate solutions.* Superconductor Science and Technology, 2012. **25**(12): p. 123001.

[6]   Matsumoto, K. and P. Mele, *Artificial pinning center technology to enhance vortex pinning in YBCO coated conductors.* Superconductor Science and Technology, 2009. **23**(1): p. 014001.

[7]   Macmanus-Driscoll, J.L., et al., *Strongly enhanced current densities in superconducting coated conductors of YBa2Cu3O7-x+BaZrO3.* Nature Materials, 2004. **3**(7): p. 439-443.

[8]   Wu, J. and J. Shi, *Interactive modeling-synthesis-characterization approach towards controllable in situ self-assembly of artificial pinning centers in RE-123 films.* Superconductor Science & Technology, 2017. **30**(10): p. 103002.

[9]   Baca, F., et al., *Control of BaZrO 3 nanorod alignment in YBa 2 Cu 3 O 7− x thin films by microstructural modulation.* Applied Physics Letters, 2009. **94**(10): p. 102512.

[10]   Baca, F.J., et al., *Interactive Growth Effects of Rare-Earth Nanoparticles on Nanorod Formation in YBa2Cu3Ox Thin Films.* Advanced Functional Materials, 2013. **23**(38): p. 4826-4831.

[11]   Emergo, R., et al., *The effect of thickness and substrate tilt on the BZO splay and superconducting properties of YBa2Cu3O7− δ films.* Superconductor Science and Technology, 2010. **23**(11): p. 115010.

[12]   Feldmann, D., et al., *Improved flux pinning in YBa2Cu3O7 with nanorods of the double perovskite Ba2YNbO6.* Superconductor Science and Technology, 2010. **23**(9): p. 095004.

[13]   Goyal, A., et al., *Irradiation-free, columnar defects comprised of self-assembled nanodots and nanorods resulting in strongly enhanced flux-pinning in YBa2Cu3O7− δ films.* Superconductor Science and Technology, 2005. **18**(11): p. 1533.

[14]   Harrington, S., et al., *Self-assembled, rare earth tantalate pyrochlore nanoparticles for superior flux pinning in YBa2Cu3O7− δ films.* Superconductor Science and Technology, 2008. **22**(2): p. 022001.

[15]   Mele, P., et al., *Ultra-high flux pinning properties of BaMO3-doped YBa2Cu3O7− x thin films (M= Zr, Sn).* Superconductor Science and Technology, 2008. **21**(3): p. 032002.

[16]   Varanasi, C., et al., *Thick YBa 2 Cu 3 O 7− x+ BaSnO 3 films with enhanced critical current density at high magnetic fields.* Applied Physics Letters, 2008. **93**(9): p. 092501.

[17]   Wang, X., et al., *Eliminating thickness dependence of critical current density in YBa 2 Cu 3 O 7− x films with aligned BaZrO 3 nanorods.* Journal of Applied Physics, 2010. **108**(11): p. 113911.

[18]   Wee, S.H., et al., *Formation of self-Assembled, double-perovskite, Ba2YNbO6 nanocolumns and their contribution to flux-pinning and Jc in Nb-Doped YBa2Cu3O7-δ Films.* Applied physics express, 2010. **3**(2): p. 023101.

[19]   Gautam, B., et al., *Transformational dynamics of BZO and BHO nanorods imposed by Y_2O_3 nanoparticles for improved isotropic pinning in $YBa_2Cu_3O_{7-\delta}$ thin films.* AIP Advances, 2017. **7**(7): p. 075308.

[20]   Gautam, B., et al., *Probing the effect of interface on vortex pinning efficiency of one-dimensional BaZrO3 and BaHfO3 artificial pinning centers in YBa2Cu3O7-x thin films.* Applied Physics Letters, 2018. **113**(21): p. 212602.

[21]   Cantoni, C., et al., *Strain-driven oxygen deficiency in self-assembled, nanostructured, composite oxide films.* Acs Nano, 2011. **5**(6): p. 4783-4789.

[22]   Awaji, S., et al., *High-performance irreversibility field and flux pinning force density in BaHfO3-doped GdBa2Cu3Oy tape prepared by pulsed laser deposition.* Applied Physics Express, 2015. **8**(2): p. 023101.

[23]   Cayado, P., et al., *Large critical current densities and pinning forces in CSD-grown superconducting GdBa2Cu3O7− x-BaHfO3 nanocomposite films.* Superconductor Science and Technology, 2017. **30**(9): p. 094007.

[24]   Civale, L., et al., *Angular-dependent vortex pinning mechanisms in YBa 2 Cu 3 O 7 coated conductors and thin films.* Applied Physics Letters, 2004. **84**(12): p. 2121-2123.

[25]   Engel, S., et al., *Enhanced flux pinning in Y Ba 2 Cu 3 O 7 layers by the formation of nanosized Ba Hf O 3 precipitates using the chemical deposition method.* Applied physics letters, 2007. **90**(10): p. 102505.

[26]   Foltyn, S.R., et al., *The role of interfacial defects in enhancing the critical current density of YBa2Cu3O7− δ coatings.* Superconductor Science and Technology, 2009. **22**(12):p.125002.

[27]   Gautam, B., et al., *Microscopic adaptation of BaHfO3 and Y2O3 artificial pinning centers for strong and isotropic pinning landscape in YBa2Cu3O7–x thin films.* Superconductor Science and Technology, 2018. **31**(2): p. 025008.

[28]   MacManus-Driscoll, J., et al., *Strongly enhanced current densities in superconducting coated conductors of YBa 2 Cu 3 O 7–x+ BaZrO 3.* Nature materials, 2004. **3**(7): p. 439.

[29]   Maiorov, B., et al., *Synergetic combination of different types of defect to optimize pinning landscape using BaZrO 3-doped YBa 2 Cu 3 O 7.* Nature materials, 2009. **8**(5): p. 398.

[30]   Maiorov, B., et al., *Influence of naturally grown nanoparticles at the buffer layer in the flux pinning in YBa2Cu3O7 coated conductors.* Superconductor Science and Technology, 2006. **19**(9): p. 891.

[31]   Miura, S., et al., *Characteristics of high-performance BaHfO3-doped SmBa2Cu3Oy superconducting films fabricated with a seed layer and low-temperature growth.* Superconductor Science and Technology, 2015. **28**(6): p. 065013.

[32]   Tobita, H., et al., *Fabrication of BaHfO3 doped Gd1Ba2Cu3O7− δ coated conductors with the high Ic of 85 A/cm-w under 3 T at liquid nitrogen temperature (77 K).* Superconductor Science and Technology, 2012. **25**(6): p. 062002.

[33]   Tsuruta, A., et al., *Enhancement of critical current density in the force-free sate of BaHfO3-doped multilayered SmBa2Cu3Oy film.* Japanese Journal of Applied Physics, 2014. **53**(7): p. 078003.

[34]   Chen, S., et al., *Generating mixed morphology BaZrO3 artificial pinning centers for strong and isotropic pinning in BaZrO3–Y2O3 double-doped YBCO thin films.* Superconductor Science and Technology, 2017. **30**(12): p. 125011.

[35]   Sebastian, M.A.P., et al., *Study of the flux pinning landscape of YBCO thin films with single and mixed phase additions BaMO3+ Z: M= Hf, Sn, Zr and Z= Y2O3, Y211.* IEEE Transactions on Applied Superconductivity, 2017. **27**(4): p. 1-5.

[36]   Wu, J. and J. Shi, *Interactive modeling-synthesis-characterization approach towards controllable in situ self-assembly of artificial pinning centers in RE-123 films.* Superconductor Science and Technology, 2017. **30**(10): p. 103002.

[37]   Wu, J.Z., et al., *The effect of lattice strain on the diameter of BaZrO3 nanorods in epitaxial YBa2Cu3O7− δ films.* Superconductor Science and Technology, 2014. **27**(4): p. 044010.

Acknowledgments